SAR Imaging via Spectral Estimation Methods

Stuart R. DeGraaf*
Environmental Research Institute of Michigan
P.O. Box 134001
Ann Arbor, MI 48113-4001

Abstract

This paper discusses the use of modern 2-D spectral estimation algorithms for SAR imaging. We provide a synopsis of the algorithms available, and discuss their relative merits for SAR imaging. SAR data collected of two commercial ships is used to compare the characteristics of imagery produced by a variety of 2-D spectral estimators.

1 Introduction

Synthetic aperture radar (SAR) imaging is a parameter estimation problem in which one seeks to estimate the scene reflectivity intensity vs. slant-plane location. Here we discuss the limitations of conventional Fourier imaging methods, and the rationale for employing alternative 2-D spectral estimation methods. Section 2 provides a synopsis of 2-D spectral estimation algorithms and discusses their relative merits for SAR, Section 3 compares imagery produced by these algorithms using data collected of two commercial ships by the WL-ERIM Data Collection System (DCS) SAR. Section 4 summarizes and draws conclusions.

Fourier imaging exploits the Fourier transform pair relationship between SAR signal history measurements and scene reflectivity, but exhibits two drawbacks. First, as the collection aperture is of finite size, the spatial resolution afforded by Fourier imaging is inherently limited. Typically, Taylor or Kaiser-Bessel weightings are employed to control impulse response (IPR) peak sidelobe and integrated sidelobe level. The poor resolution and/or sidelobe artifacts afforded by this tradeoff is undesirable. Second, scintillation of independent unresolved scattering elements leads to the coherent imaging speckle phenomenon.

*Sponsored by the Advanced Research Projects Agency (DOD), Advanced Systems Technology Office, under ARPA Order No. A284, issued by U.S. Army Missile Command under Contract No. DAAH01-93-C-R178. Approved for public release; distribution unlimited. Review of this material does not imply Department of Defense endorsement of factual accuracy or opinion. The author wishes to thank Wright Laboratory for providing DCS SAR data of two commercial ships.

Modern nonlinear spectral estimation methods offer the promise of improved resolution and contrast, and reduced speckle. Improvements in resolution and reductions in sidelobe artifacts arise through adaptive nulling, linear predictive modeling, and signal-noise subspace decomposition. Speckle reduction arises through the signal history domain averaging implicit in PSD image estimation. Contrast improvement arises through signal-noise subspace decomposition or algorithm singularities.

2 2-D Spectral Estimation Algorithms

In this section, we provide as synopsis of many available 2-D spectral estimation algorithms and discuss their relative advantages for SAR imaging.

Table 1 summarizes the rationale and formulation of a variety of 2-D spectral estimation algorithms. The table groups the algorithms on the basis of their rationale. Most of these algorithms are discussed in [1,2]. However, reduced-rank MVM [3], ASR [4,5], and SVA [6] are new. Moving from the top of the table toward the bottom, the degree to which the algorithms exploit a point scattering (sinusoidal signal history) model increases. While Fourier SAR imagery is often characterized by "prominent points", the point scattering model can be compromised by a variety of common physical phenomena: glints, sliding speculars, creeping waves, motion-induced phase errors, and frequency-dependent scattering amplitude such as resonances.

The mathematical notation in Table 1 is as follows. The elements of vector $\underline{X}$ are the rectangularly formatted 2-D radar signal history samples. The elements of vector $\underline{W}(r)$ are the exponential coefficients of a 2-D Fourier transform tuned to spatial location r. Diagonal matrix $\mathbf{A}$ represents a real-valued signal history weighting function used to control the tradeoff between IPR mainlobe and sidelobes. Signal history correlation matrix $\mathbf{R}$ is an estimate of the expected matrix $E(\underline{X}\underline{X}^H)$. We employ forward-backward subaperture averaging, i.e. the modified covariance method, to

1058-6393/95 $4.00 © 1995 IEEE

Technique	Rationale	PSD or Coherent Spectrum
FFT	non-adaptive filterbank	$\underline{W}^H(r)\mathbf{A}\underline{X}$
ASR/SVA	adaptive filterbank	adaptively FIR filter $\underline{W}^H(r)\underline{X}$
periodogram	non-adaptive filterbank expected output energy	$\underline{W}^H(r)\mathbf{ARA}\underline{W}(r)$
RRMVM	reduced-rank MVM	$\frac{\underline{W}^H(r)(\mu(r)\mathbf{I}+\mathbf{R})^{-1}\mathbf{R}(\mu(r)\mathbf{I}+\mathbf{R})^{-1}\underline{W}(r)}{(\underline{W}^H(r)(\mu(r)\mathbf{I}+\mathbf{R})^{-1}\underline{W}(r))^2}$
MVM	adaptive filterbank expected output energy	$\frac{1}{\underline{W}^H(r)\mathbf{R}^{-1}\underline{W}(r)}$
ARLP	linear data extrapolation AR system driven by white noise	$\frac{\sqrt{R^{-1}_{P,P}}}{\lvert\underline{P}^H\mathbf{R}^{-1}\underline{W}(r)\rvert}$
Pisarenko	RMS average over prediction element of reciprocal ARLP spectra	$\frac{1}{\sqrt{\underline{W}^H(r)\mathbf{R}^{-2}\underline{W}(r)}}$
EV/MUSIC	signal-noise subspace decomposition within MVM framework	$\frac{1}{\underline{W}^H(r)(\sum_{noise}\lambda_m^{-1}\underline{V}_m\underline{V}_m^H)\underline{W}(r)}$ or $\frac{1}{\underline{W}^H(r)(\sum_{noise}\sigma_o^{-2}\underline{V}_m\underline{V}_m^H)\underline{W}(r)}$

Table 1: Synopsis of 2-D spectral estimation algorithm rationale and formulation.

estimate the signal history correlation matrix. $\{\lambda_m\}$ and $\{\underline{V}_m\}$ represent the eigenvalues and orthonormal eigenvectors, respectively, of $\mathbf{R}$. Prediction indicator vector $\underline{P}$ has a one in the P^{th} element, the signal history element being predicted, and zeros elsewhere.

The Fourier transform (FFT) and adaptive sidelobe reduction (ASR) algorithm produce coherent (complex-valued) spectra. These coherent images represent the outputs of banks of 2-D narrowband filters, where each filter output is tuned to a given spatial location. The FFT filters are fixed, while the ASR filters are adaptive. In other words, the FFT IPR is space-invariant, while the ASR IPR is space-variant. One computes the ASR image by applying a space-variant FIR filter to a uniformly weighted (sinc IPR) Fourier image, and chooses the ASR filter coefficients to maximize the output signal-to-interference-ratio (SIR) in a single-realization sense [4,5]. Both separable and nonseparable 2-D implementations are available, as are over and under determined versions; for a given order, the nonseparable filter provides more adaptive degrees of freedom. Space-variant apodization (SVA) [6] is a special case of overdetermined ASR that employs a single degree of freedom, together with a constraint motivated by the oscillatory nature of the sidelobes of a sinc IPR.

The periodogram, minimum variance method (MVM), and reduced-rank MVM (RRMVM) produce power spectral density (positive semi-definite, real-valued) spectra. These PSD images represent the average, or expected value, of the output energies of banks of 2-D narrowband filters, where each filter output is tuned to a given spatial location. The periodogram filters are fixed, while MVM and RRMVM filters are adaptive. In each case, a correlation matrix $\mathbf{R}$, whose entries are an estimate of the correlations between signal history domain data samples, must be estimated from the signal history data. Both MVM and RRMVM compute narrowband filters that maximize the output SIR in an expected or average sense. MVM requires a full-rank, nonsingular correlation matrix estimate, which implies a large amount of averaging, while RRMVM accommodates a reduced-rank, singular correlation matrix based on a small amount of averaging.

ASR and RRMVM share the spirit of MVM in that they seek to maximize SIR. However, both are "singular" methods in that they optimize SIR on the basis of singular signal history correlation matrices. Consequently, these algorithms impose a constraint on the l_2 norm of the weighting vector to insure non-zero output. Choice of the constraint value controls the behavior of the algorithms.

AutoRegressive Linear Prediction (ARLP) methods predict signal history samples as linear combinations of the neighboring signal history samples, and select the predictor filter coefficients to minimize average prediction error. Treating the prediction error (assumed white) as the excitation of an autoregressive prediction filter, the PSD estimate equals the minimized prediction error energy divided by the magnitude squared of the transfer function. However, it is known that the PSD should be chosen as the square root of this quantity to obtain correct scaling. ARLP imagery based on any one choice of prediction element may exhibit spiky behavior and elliptical, rather than circular, contours. To reduce these undesirable properties, one can form an average image based on multiple prediction elements. In particular, one can evaluate an RMS average ARLP image, whose inverse is the RMS average of the inverse ARLP images yielded by all possible prediction elements. If one assumes *a-priori* that the individual ARLP filters yield the same prediction error energy, then the RMS ARLP image reduces to one of Pisarenko's [7] spectral estimates.

EigenVector (EV) and MUltiple SIgnal Classification (MUSIC) methods can be viewed as variants of the MVM spectrum that cause the image peaks corresponding to high-TCR point scatterers to become very sharp and high (tending toward infinity). The rationale for these methods is that the eigenvectors of **R** that span the noise subspace are orthogonal to signal vectors corresponding to prominent point scatterers. The height of EV and MUSIC peaks is a measure of "pointiness" rather than of scattering intensity. EV and MUSIC methods differ in that MUSIC explicitly whitens, or equalizes, the noise eigenvalues, while EV does not. Explicit whitening destroys the spatial inhomogeneities associated with terrain clutter or other diffuse scattering in SAR imagery; thus MUSIC is not generally suitable for SAR imaging. In contrast, the EV method preserves the clutter inhomogeneities, while smoothing speckle, and enhancing the sharpness and contrast of prominent point scatterers.

Two other methods are well suited to specialized applications in which accurate localization of point scatterers is of paramount importance: Tufts-Kumaresan ARLP and parametric maximum likelihood. In our experience, neither of these algorithms is well suited to general SAR imaging.

For reasonable choices of filter order or degree of averaging, ASR and RRMVM enjoy a considerable computational advantage over the other adaptive methods, which involve inversion or eigen decomposition of a full-rank correlation matrix. For a $K \times K$ signal history, the computational complexity of ASR and MVM are $O(K^2 \log K)$, while that of the other methods is K^6. For perspective, K is often on the order of 1000. In practice, it is necessary to employ a decimation and mosaicing strategy to apply the latter algorithms to typical SAR scenes.

3 Collected Scalar SAR Results

Here, we utilize Ku-band data collected by the WL-ERIM DCS radar of two commercial ships docked near Toledo, OH, together with some calibration trihedrals, to compare the benefits and limitations of the various algorithms algorithms for SAR imaging. The same signal history, which affords a uniformly weighted (sinc IPR) Fourier image resolution of one meter, was used to produce all images shown. We exploited signal history decimation and image mosaicing to compute MVM, ARLP, Pisarenko, and EV images based on 40% subaperture forward-backward averaging.

Fig. 1a illustrates the baseline Taylor-weighted (-35dB peak sidelobe, order 5) Fourier image on a relative 60dB grayscale. Sidelobes are visible in the water from the trihedral near the water's edge. All subsequent images should be compared against this baseline.

Fig. 1b illustrates the MVM image on a relative 45dB scale. The reduced dynamic range was chosen to preserve the apparent contrast ratio. Diminished compression gain afforded by the 40% subapertures used accounts for 8dB of the difference; we hypothesize that along-track phase errors, together with MVM's increased sensitivity to such errors, accounts for the remaining 7dB loss of contrast. Contrast aside, MVM improves the sharpness of the trihedrals (by roughly a factor of 7 at the 3dB point) and resolution of detail on the ships, yet displays less IPR scintillation (breakup) along the continuous bulkheads and gunwales of the ships. The MVM image displays no sidelobe artifacts and reduces clutter speckle. The MVM image has a more "optical" quality than the Fourier image.

Fig. 1c illustrates the RRMVM image, evaluated using a forward-backward subaperture size of 400 (out of 402) samples and a constraint of 1.002, on a relative 70dB scale. This example highlights a problem that can arise with RRMVM when a large dynamic range of scattering amplitudes exists within the scene. In this case, RRMVM eliminates much of the detail of the ships' structure between the bow and stern, yet, at the same time, fails to eliminate the sidelobes of the bright trihedral scatterers. To first order, the effect of RRMVM is to threshold the uniformly-weighted (sinc IPR) Fourier image. RRMVM exhibits too many adaptive degrees of freedom for the small amount of averaging and highly singular correlation matrix employed. The result is global weak signal suppression.

Fig. 1e illustrates the nonseparable (order 2, constraint .5) ASR image on a relative 70dB grayscale. Sidelobes are no longer visible in the water from the trihedral near the water's edge despite the 10dB increased dynamic range of the ASR display. The trihedrals and prominent scatterers on the ships are more sharply defined. Slices through the trihedrals demonstrate that the ASR "mainlobe" is slightly sharper than a corresponding sinc IPR. In addition the contrast of the trihedrals with respect to the surrounding clutter is improved by roughly 8dB, although the variance of the clutter speckle (on a dB scale) is increased. While the ASR image eliminates sidelobes without suppressing weak scatterers globally, it does suppress weak scatterers locally, on the scale of the FIR filter size. Clutter suppression, local weak signal suppression, and increased clutter speckle are related phenomena caused by the complete lack of averaging in the underdetermined spectral estimate, despite the small number of adaptive degrees of freedom.

Fig. 1d illustrates the SVA image on a relative 60dB grayscale. Sidelobes are no longer visible in the water from the trihedral near the water's edge, yet the trihedrals and prominent scatterers on the ships are more sharply defined. For comparison, Fig. 1e illustrates the unweighted (sinc IPR) Fourier image on a relative 60dB grayscale. Clearly, the dominant impact of SVA is to eliminate the sidelobe artifacts while leaving the sinc IPR mainlobe and clutter largely intact. Slices through the trihedrals demonstrate that the SVA and sinc "mainlobes" are virtually identical.

Fig. 1f illustrates the ARLP image on a relative 35dB scale. The reciprocal of this image is the RMS average of two reciprocal ARLP images based on first- and second-quadrant predictors. The ARLP image looks qualitatively rather poor. Compared to the MVM image, the ARLP image offers less contrast, displays spurious diagonal texture, and exhibits sidelobe-like artifacts that extend throughout the scene.

Fig. 1g illustrates the Pisarenko image on a relative 35dB scale. Compared to the MVM image, Pisarenko loses roughly 10dB of compression gain or contrast. We suspect this occurs because Pisarenko is even more sensitive than MVM to along-track phase errors. Otherwise, there appears to be little difference between the Pisarenko and MVM imagery. However, by averaging over all possible ARLP predictors, the Pisarenko image greatly reduces the spurious diagonal texture and improves the contrast afforded by the ARLP image based on a pair of prediction elements.

Fig. 1h illustrates the EV image on a relative 45dB scale. We used a simple energy-based order selection criterion, wherein the order is chosen so that the sum of the signal (largest) eigenvalues equals 90% of the sum of all the eigenvalues. Compared to the MVM image, EV gains roughly 5dB of contrast, and appears strikingly sharp. The EV image is pleasing in mosaic chips that include either man-made objects or inhomogeneous clutter. In such cases our order selection criterion enhances prominent points and meaningful texture with respect to benign homogeneous regions, which are smoothed as with MVM. However, the EV image exacerbates random noise texture in mosaic chips comprised of homogeneous clutter; in such cases there are no dominant signal eigenvalues, yet the order selection criterion decrees some to be signal, and EV enhances the associated points. Order selection criteria that are based solely on discontinuities in or thresholding of the eigenvalue spectrum fail to satisfy our desire to enhance scatterers on the basis of their local prominence or relative spatial position. Order selection is complicated by the arbitrary manner in which an object or terrain can span multiple mosaic chips. More sophisticated order selection criteria are necessary to fully realize the potential of EV for SAR imaging.

4 Conclusions

This paper discussed the rationale for using modern 2-D spectral estimation algorithms, rather than Fourier transforms, to form SAR imagery, and provided examples of their application to collected SAR data. Of the methods discussed here, the methods that seem to offer the most immediate utility are MVM, Pisarenko, ASR and SVA. MVM and Pisarenko offer improved resolution of prominent scatterers, reduced speckle, and imagery that is more "optical" in character than Fourier imagery. Pisarenko's method produces cleaner imagery than conventional ARLP by averaging over all possible prediction elements. SVA offers sinc-like resolution without sidelobe artifacts; ASR offers slightly sharper resolution as well as TCR gain, albeit at the cost of increased speckle. The computational burden of SVA and ASR is trivial compared with that of MVM and Pisarenko. EV offers great potential for enhancing resolution and contrast in SAR imagery; however, sophisticated new methods for estimating model order, based on local spatial content, rather than simply intensity, must be developed before EV can realize its full potential.

References

[1] S. M. Kay, *Modern Spectral Estimation Theory and Application*, Prentice-Hall, Englewood Cliffs, 1988.

[2] S. L. Marple, Jr., *Digital Spectral Analysis with Applications*, Prentice-Hall, Englewood Cliffs, 1987.

[3] G. R. Benitz, "Preliminary Results in Adaptive High Definition Imaging for Stationary Targets," *MIT Lincoln Laboratory Project Report AST-34*, Nov. 1993.

[4] S. R. DeGraaf, "Sidelobe Reduction via Adaptive FIR Filtering in SAR Imagery", *IEEE Trans. on Image Proc.*, vol. 3, no. 3, May 1994.

[5] S. R. DeGraaf, "SAR Imaging via Modern 2-D Spectral Estimation Methods", Proc. 1994 SPIE Workshop, Algorithms for Synthetic Aperture Radar, Orlando, FL, May 1994.

[6] H. C. Stankwitz, R. J. Dallaire, J. R. Fienup, "Non-linear Apodization for Sidelobe Control in SAR Imagery", to appear in *IEEE Trans. Aerosp., Elec. Sys.*, January, 1995.

[7] V. F. Pisarenko, "On Estimation of Spectra by Means of Nonlinear Function of the Covariance Matrix", *Geophys. J. Roy. Astron. Soc.*, vol. 28, 1972, pp. 511-531.

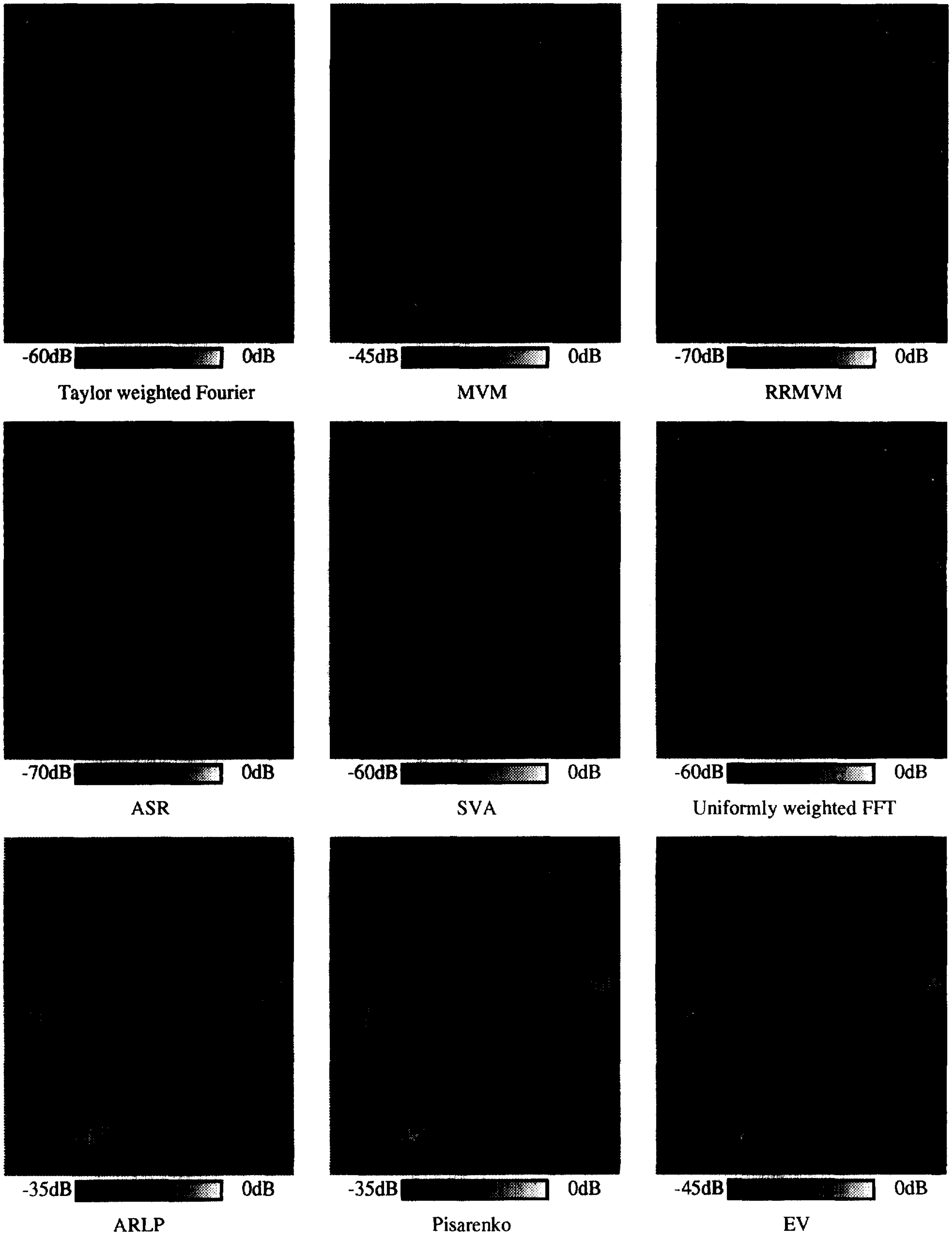

Figure 1: Comparison of SAR imagery produced by different spectral estimators.